

Fernando Alonso Marroquín and Hans Herrmann

(*) *ICA1, University of Stuttgart,
Pfaffenwaldring 27, 70569 Stuttgart, Germany*

Stefan Luding^(*)

*Technische Universiteit Delft (TUD),
DelftChemTech, Particle Technology,
Julianalaan 136, 2628 BL Delft, The Netherlands
(July 25, 2002)*

We investigate the constitutive response of two-dimensional packed samples of polygons using molecular dynamics simulation. The incremental elasto-plastic response is examined in the pre-failure regime. Besides the Young modulus and the Poisson ratio, an additional parameter must be included, which takes into account the anisotropy of the elastic response. The plastic deformations are described by the introduction of the yield and the flow directions. These directions do not agree, which reproduces the non-associated feature of realistic soils. In order to detect the yield surface, different loading-unloading-reloading tests were performed. During the reload path, it is found that the yielding develops continuously with the amplitude of loading, which does not allow to identify a purely elastic regime.

I. INTRODUCTION

Traditionally, the quasi-static deformation of soils has been described by using constitutive laws. They are empirical relations between the stress and the strain involving a certain number of material parameters, which, in the simplest models, can be measured in experimental tests [1–3]. However, the more sophisticated models involve so many parameters that their direct experimental meaning and their identification becomes impossible.

In the last years the numerical simulations have been used as an alternative to study the behavior of soils. Usually, disks or spheres are used in order to capture the granularity of the materials [4–7]. The simplicity of their geometry allows to reduce the computer time of calculations. However, they do not take into account the diversity of shapes of the grains in realistic materials.

A more detailed description is presented here by using randomly generated convex polygons. The interaction between the polygons can be handled by letting the polygons interpenetrate each other and calculating the force as a function of their overlap [8]. This approach has been successfully applied to model different processes, like fragmentation [9,11], damage [12,10], strain localization and earthquakes [8]. The contribution of this work is to determine the constitutive relation of this discrete model material in the regime of quasi-static deformations. The results show that simple mechanical laws at the grain level are able to reproduce the complex macroscopic behavior of the deformation of soils.

The details of the particle model are presented in Sec. II. In addition to the normal contact force mentioned above, the tangential contact force law is implemented by a Coulomb friction criterion, and the boundary condi-

tions are modeled by the introduction of a flexible membrane that allows to fix the stress value. The calculation of the constitutive relations is presented in Sec. III. We discuss the results in the framework of the classical theory of elasto-plasticity. The summary and the perspectives of this work are presented in Sec. IV.

II. MODEL

The polygons representing the particles of this model are generated using a simple version of the Voronoi tessellation: First, we choose a random point in each cell of a regular square lattice, then each polygon is constructed assigning to each point that part of the plane that is nearer to it than to any other point. Each polygon is subjected to interparticle contact forces and boundary forces as we explain below.

When two polygons overlap, two contact points appear form the intersection of their edges. The contact line is defined by the segment connecting these two intersection points. The contact force is calculated as

$$\vec{f}^c = k_n \Delta x_n^c \hat{n}^c + k_t \Delta x_t^c \hat{t}^c, \quad (1)$$

here \hat{n}^c and \hat{t}^c denotes the normal and tangential unitary vectors with respect to the contact line, and k_n and k_t are the stiffness in the respective directions. The overlapping length Δx_n^c is the ratio between the overlap area of the polygons and the length of their contact line. Δx_t^c defines the elastic tangential displacement of the contact, that is given by the time integral starting at the begin of the contact

$$\Delta x_t^c = \int_0^t v_t^c(t') \Theta(f_t^c - \mu f_n^c) dt', \quad (2)$$

Where Θ is the Heaviside function and \vec{v}_i^c denotes the tangential component of the relative velocity \vec{v}^c at the contact. \vec{v}^c depends on the linear velocity \vec{v}_i and angular velocity $\vec{\omega}_i$ of the particles in contact according to

$$\vec{v}^c = \vec{v}_i - \vec{v}_j - \vec{\omega}_i \times \vec{\ell}_i + \vec{\omega}_j \times \vec{\ell}_j. \quad (3)$$

The branch vector $\vec{\ell}_i$ connects the center of mass of particle i with the point of application of the contact force. This point is taken as the center of mass of the overlapping polygon. Eq. (2) defines a limit of elasticity in the contact force. When the contact force satisfies $f_t^c = \mu f_n^c$ the contact slips, giving rise to a plastic deformation.

The external forces are applied on the boundary through a flexible membrane which surrounds the sample. Such a membrane is calculated using an iterative algorithm, that selects the segments of the external contour whose bending angle is smaller than a threshold angle θ_{th} [13]. On each selected segment $\vec{T} = \Delta x_1 \hat{x}_1 + \Delta x_3 \hat{x}_3$, we apply an external force of the form

$$\vec{f}^b = -\sigma_1 \Delta x_3 \hat{x}_1 + \sigma_3 \Delta x_1 \hat{x}_3. \quad (4)$$

Here \hat{x}_1 and \hat{x}_3 are the unit vectors of the Cartesian coordinate system. σ_1 and σ_3 are the components of the stress we want to apply on the sample, as it is presented in Sec. III.

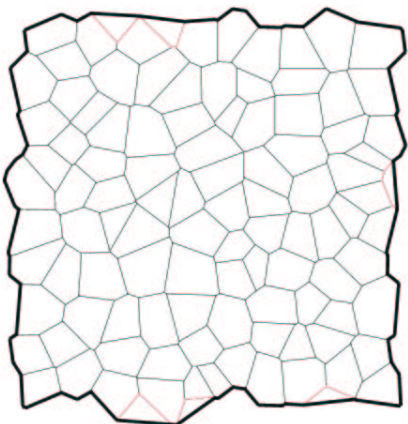


FIG. 1. Schematic plot of the membrane obtained with threshold bending angle $\pi/2$.

The contact forces and the boundary forces are inserted in Newton's equations of motion which is solved numerically using a predictor-corrector algorithm. In order to enhance the stability of the numerical method and to allow for rapid relaxation, some viscous forces are included both in the contacts and in the boundaries:

$$\begin{aligned} \vec{f}_v^c &= -m(\gamma_n v_n^c \hat{n}^c + \gamma_t v_t^c \hat{t}^c), \\ \vec{f}_v^b &= -m_i \gamma_t \vec{v}_i. \end{aligned} \quad (5)$$

The contribution of these forces is almost negligible in the quasi-static regime where velocities are small. They

are included only to reduce the acoustic waves emitted when the system goes from one equilibrium state to the other. $m = (1/m_i + 1/m_j)^{-1}$ is the effective mass of the particles in contact, and m_i is the mass of the particle i in contact with the membrane.

There are three characteristic times in the simulation: The relaxation time $t_r = 1/\gamma_n$, the loading time t_0 and the characteristic period of oscillation $t_s = \sqrt{k_n/m_0}$. Here m_0 is the mean mass of the polygons. This leads to a minimum set of dimensionless parameters, whose selected values are shown in the table.

variable	ratio	default value
time of relaxation	t_r/t_s	0.1
time of loading	t_0/t_s	1250
friction coefficient	μ	0.25
stiffness ratio	$k_t/k_n = \gamma_t/\gamma_n$	0.33
bending angle	θ_{th}	$\pi/4$

III. CONTINUOUS RELATIONS

The characterization of the macroscopic state of a granular material in static equilibrium is usually given by the Cauchy stress tensor. The derivation of this tensor over a representative volume [14] leads to

$$\sigma_{ij} = \frac{1}{A} \sum_b x_i^b f_j^b. \quad (6)$$

The sub-scripts i and j in Eq. (6) denote the components of vectors and tensors. Here \vec{x}^b is the point of application of the boundary force \vec{f}^b . This force is defined in Eq. (4). A is the area enclosed by the boundary. The sum goes over all the boundary forces of the sample. Inserting Eq. (4) in Eq. (6) leads to

$$\sigma = \frac{1}{A} \begin{bmatrix} -\sigma_1 \sum_b x^b \Delta y^b & \sigma_3 \sum_b x^b \Delta x^b \\ -\sigma_1 \sum_b y^b \Delta y^b & \sigma_3 \sum_b y^b \Delta x^b \end{bmatrix}. \quad (7)$$

These sums can be converted into integrals over closed loops. Then, the calculation of such integrals leads to

$$\sigma = \begin{bmatrix} \sigma_1 & 0 \\ 0 & \sigma_3 \end{bmatrix}. \quad (8)$$

Thus, the stress eigensystem coincides with the Cartesian coordinate system used. We can reduce the notation introducing the *pressure* p and the *shear stress* q in the components of the *stress vector*

$$\vec{\sigma} = \begin{bmatrix} p \\ q \end{bmatrix} = \frac{1}{2} \begin{bmatrix} \sigma_1 + \sigma_3 \\ \sigma_1 - \sigma_3 \end{bmatrix}. \quad (9)$$

In the same way, the incremental strain tensor can be calculated as the average of the displacement gradient over the area of the sample. It has been shown [15] that

this average can be transformed into a sum over boundary segments of the sample

$$d\epsilon_{ij} = \frac{1}{A} \sum_b \Delta x_i^b N_j^b. \quad (10)$$

Here N^b is the 90° counterclockwise rotation of the boundary segment \vec{T} . The displacement of the segment $\Delta \vec{x}^b$ is calculated from the linear displacement $\Delta \vec{x}$ and the angular rotation $\Delta \vec{\phi}$ of the polygon, according to

$$\Delta \vec{x}^b = \Delta \vec{x} + \Delta \vec{\phi} \times \vec{\ell}. \quad (11)$$

The vector $\vec{\ell}$ connects the center of the segment with the center of mass of the polygon to which it belongs.

The eigenvalues $d\epsilon_1$, $d\epsilon_3$ of the symmetric part of $d\epsilon_{ij}$ define the *volumetric* and *shear* component of the strain as the components of the *incremental strain vector*:

$$d\tilde{\epsilon} = \begin{bmatrix} d\epsilon_v \\ d\epsilon_\gamma \end{bmatrix} = \begin{bmatrix} d\epsilon_1 + d\epsilon_3 \\ d\epsilon_1 - d\epsilon_3 \end{bmatrix}. \quad (12)$$

From the **macro-mechanic** point of view, each state of the sample is related to a single point in the stress space, and the quasi-static evolution of the system is represented by the movement of this point in the stress space. The resulting deformation during the transition from stress state $\tilde{\sigma}$ to $\tilde{\sigma} + d\tilde{\sigma}$ is given by the incremental strain $d\tilde{\epsilon}$. In advance, let us separate the incremental stress in its *elastic* (recoverable) and *plastic* (irrecoverable) components:

$$d\tilde{\epsilon} = d\tilde{\epsilon}^e + d\tilde{\epsilon}^p. \quad (13)$$

Following the procedure proposed by Bardet [7] both components can be obtained as it is shown in Fig. 2. Initially, the sample is in the stress state $\tilde{\sigma}$. Loading the sample from $\tilde{\sigma}$ to $\tilde{\sigma} + d\tilde{\sigma}$ the strain increment $d\tilde{\epsilon}$ is obtained. Then the sample is unloaded, back to the original $\tilde{\sigma}$, and one finds a remaining strain $d\tilde{\epsilon}^p$, that corresponds to the plastic component of the incremental strain. For small stress increments the unloaded stress-strain path is almost elastic. Thus, the difference $d\tilde{\epsilon}^e = d\tilde{\epsilon} - d\tilde{\epsilon}^p$ can be taken as the elastic component of the strain.

This procedure is implemented on one sample choosing different stress directions. Fig. 2 shows the load-unload stress paths and the corresponding strain response when an initial stress state with $q = p/4$ is chosen, corresponding to $\sigma_1 = 5p/4$ and $\sigma_3 = 3p/4$, a larger stress in vertical direction. The end of the load paths in the stress space maps into a strain envelope response $d\tilde{\epsilon}(\theta)$ in the strain space. Likewise, the end of the unload paths map into a plastic envelope response $d\tilde{\epsilon}^p(\theta)$. The *yield direction* ϕ can be found from this response, as the direction in the stress space where the plastic response is maximal. This is close to $\theta = 90^\circ$ in this case. The *flow direction* ψ is given by the direction of the maximal plastic response in the strain space, which is close to 70° in this example. We found that these directions do not agree, corresponding

to a *non-associated flow rule* as it is observed in experiments on realistic soils [17]. If one approximates the plastic envelope response by its projection in the flow direction, the elastic response can be written as the simple form

$$d\tilde{\epsilon}^p = \frac{\langle \hat{\phi} \cdot d\tilde{\sigma} \rangle}{h} \hat{\psi}. \quad (14)$$

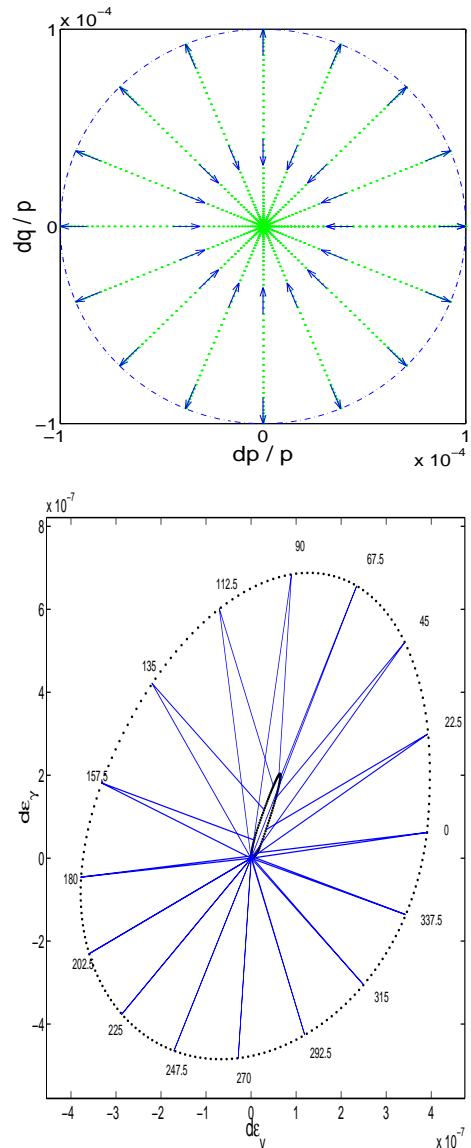


FIG. 2. Stress- and strain-relations resulting from the load-unload test. grey lines represent the paths in the stress and strain spaces. The dotted line gives the strain envelope response and the solid line is the plastic envelope response.

The so-called *hardening modulus* h is the ratio between the modulus of the maximal plastic strain and the modulus of the incremental stress. The function $\langle x \rangle$ is defined as zero if $x \leq 0$; Otherwise it is valued to x . The unit vectors $\hat{\psi}$ and $\hat{\phi}$ define the flow direction and the yield direction, respectively. The vector $d\tilde{\sigma}$ defines the direction and magnitude of applied load.

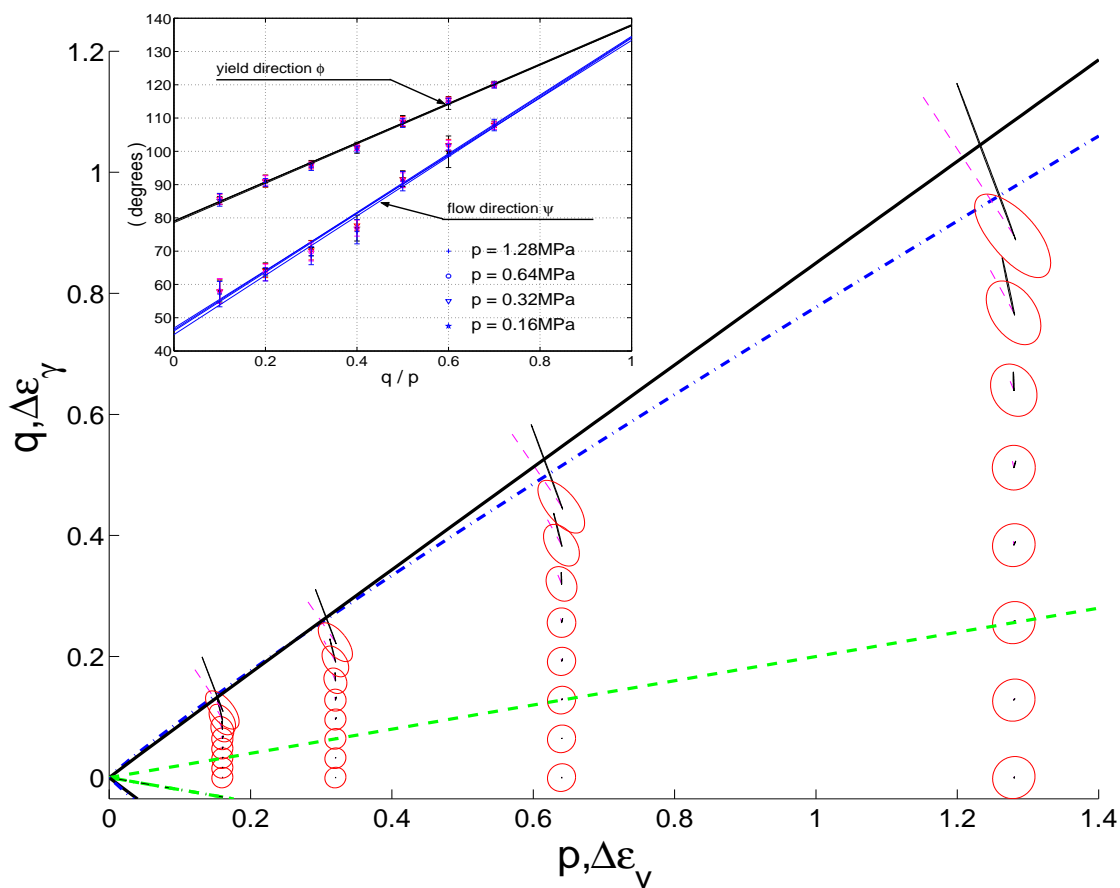


FIG. 3. Elastic response $d\tilde{\epsilon}^e$ and plastic response $d\tilde{\epsilon}^p$ for different levels of pressure p and shear stress q . The envelope responses result from the application of different loading modes with $|d\tilde{\sigma}| = 10^{-4}p$. The elastic response, calculated from Eq. (13), has a centered ellipse as envelope response. The plastic strain response lies almost on a straight line oriented in the flow direction. This direction does not correspond with the yield direction (dashed lines). The dash-dotted line represents the failure surface. When a stress value above this line is applied the system fails. The solid line represents the plastic limit surface. The latter is obtained connecting the points where the plastic deformation diverges. (That means $d\tilde{\epsilon}^p/|d\tilde{\sigma}| \rightarrow \infty$) The dashed line $q = 0.18p$ represents the limit of the zone where the isotropic elasticity assumption is valid. The plot shows the yield and the flow directions as a function of the deviatoric stress ratio q/p , evaluated from the average over five different samples. These calculations are made with fixed $k_n = 160$ MPa.

Both elastic and plastic envelope responses are calculated from different stress values. The results are shown in Fig. 3. The elastic response, calculated from Eq. (13), has a centered ellipse as envelope response for all the cases. Since the direction of this response does not always correspond to the direction of the volumetric strain increment, the general form for the elastic stiffness must be written as

$$d\tilde{\epsilon}^e = \frac{2}{E} \begin{bmatrix} 1 - \nu & -\alpha \\ -\alpha & 1 + \nu \end{bmatrix} d\tilde{\sigma}. \quad (15)$$

Here E and ν are the classical parameters of the elasticity, i.e. the Young modulus and the Poisson ratio. They are not material parameters because they depend on the stress state we take. Moreover, an additional variable α must be included in this relation, taking into account the anisotropy of the elastic response. A limit of isotropy is found around $q = 0.18p$ (See Fig. 3). Below of this line

the parameters of elasticity are almost constants with $\alpha \approx 0$. Above this limit the stiffness decreases as a result of open contacts, giving rise to an anisotropic elastic response.

In a previous work [13], the elasto-plastic quantities resulting from Eq. (14) and Eq. (15) have been evaluated as a function of the stress state. Since the mechanical response of soils depends not only on the initial stress state but also on the way how this state is reached [16], these results are only valid in the case of monotonic load. In the classical theory of elasto-plasticity, the dependence of the strain response on the history of the deformation is described by the evolution of the so-called *yield surface*. This surface encloses a hypothetical region in the stress space where only elastic deformations are possible [18].

We attempt to detect the yield surface by using a standard procedure proposed in experiments with sand [17]. Fig. 4 shows this procedure: initially the sample is sub-

ject to isotropic pressure. Then the sample is loaded in the axial direction until it reaches a yield-stress state with pressure p and shear stress q . Since plastic deformation is found in this stress value, the point (p, q) can be considered as a classical yield point. Then, the classical theory assumes the existence of a yield surface containing this point. In order to explore the yield surface, the sample is unloaded in the axial direction until it reaches the stress point with pressure $p - \delta p$ and shear stress $q - \delta q$ inside the elastic regime. Then the yield surface is constructed by taking different directions in the stress space for re-loading. In each direction, the new yield point must be detected by a sharp change in the slope in the stress-strain curve, indicating plastic deformations.

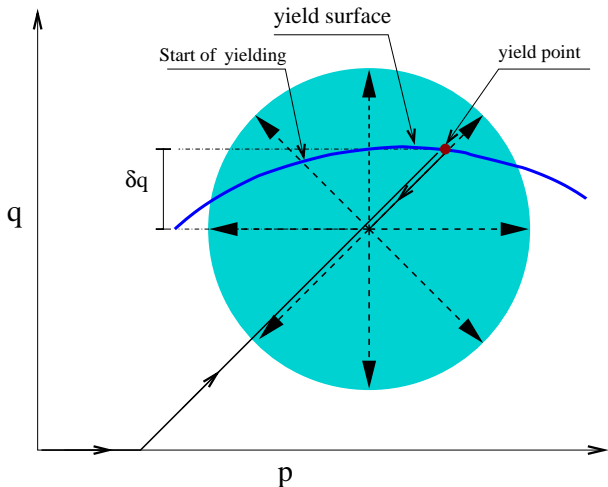


FIG. 4. Experimental procedure used to obtain the yield surface. Load-unload-reload tests are performed, and the points in the reload path, where the yielding begins are marked. The yield function is constructed by connecting these points.

Fig. 5 shows the strain response taking different load directions in the same sample. If the direction of the reload path is the same as that one of the original load (45°), we observe a sharp decrease of stiffness when the load point reaches the initial yield point, which corresponds to the origin in Fig. 5. However, if we take a different direction of re-loading, we find that the decrease of the stiffness with the loading becomes smooth. Since there is no straightforward way to identify those points where the yielding begins, the yield function, as it was introduced by Drucker & Prager [18] in order to describe a sharp transition between the elastic and plastic regions is not consistent with our results.

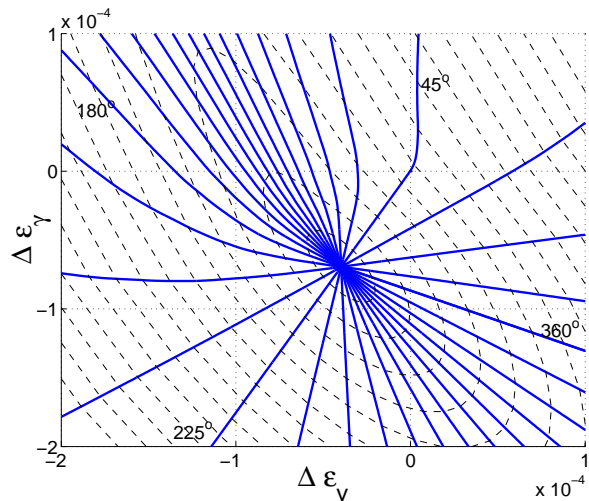


FIG. 5. Strain response resulting from the preparation of the sample according to Fig. 4. The solid lines show the strain response for different loading directions. The dashed contours connect the strain increments values with the same value of $|\Delta\tilde{\sigma}|$. The Figure shows that in any reload path different to that one of the original load the yielding develops continuously. Thus, it is not possible to distinguish an elastic regime.

IV. CONCLUDING REMARKS

The incremental elasto-plastic response of a Voronoi tessellated sample of polygons has been examined in the framework of the classical theory. The resulting constitutive relation leads to non-linear, anisotropic elasticity, where the classical parameters of elasticity, the Young modulus and the Poisson ratio, are not material constants. The plastic response reflects the non-associated features of realistic soils. Here the classical analysis of Drucker & Prager is not applicable, because it is not possible to determine an elastic regime.

Future work will be oriented to a micro-mechanically based description of these elasto-plastic features. Since the mechanical response of the granular sample is represented as a collective response of all the contacts, it is expected that the macro-mechanical response can be completely characterized by the inclusion of some field-variables, which contain the information about the micro-structural arrangements between the grains. Some statistical variables like the fabric tensor have been included as internal variables [6,19]. This description, however, does not seem to offer a complete characterization of the constitutive response. More salient aspects, such as the yielding of the contacts, and the fluctuations of the stress inside the granular material, might offer a more complete set of internal variables for the description of the macroscopic state. This is, in our point of view, an important challenge in the future.

We thank F. Darve, P. Vermeer, F. Kun, and J. Åstrøm for helpful discussions and acknowledge the support of the *Deutsche Forschungsgemeinschaft* within the research group *Modellierung kohäsiver Reibungsmaterialien*.

-
- [1] P. A. Vermeer, "A five-constant model unifying well-established concepts" in *Constitutive Relations of soils*, edited by G. Gudehus, F. Darve and L. Vardoulakis, Balkema Rotterdam, 175-197 (1984)
- [2] F. Darve, "Incremental non-linear constitutive relationships" in *Geomaterials Constitutive Equations and Modeling*, edited by F. Darve, Elsevier applied Science, London 123-148 (1990)
- [3] D. Kolymbas "An outline of hypoplasticity" *Arch. App. Mech.* **61**, 143-154 (1991)
- [4] P.A Cundall, "Numerical experiments on localization in frictional materials" *Ingenieur-Archiv*, **59** 879-908 (1989)
- [5] F. Radjai, M. Jean, J.J. Moreau and S. Roux "Force distributions in Dense Two Granular systems" *Phys. Rev. Lett.* **77**, 2 274-277 (1996)
- [6] C. Thornton *Computer simulated deformation of compact granular assemblies* *Acta Mechanica* **64**, 45-61 (1986)
- [7] J.P. Bardet, "Numerical solutions of incremental response of idealized granular materials" *Int. J. Plasticity* **10**(8) 879-908 (1994)
- [8] H. Tillemans and H.J. Herrmann, "Simulating deformations of granular solid under shear" *Phys. A* **217**, 261-288 (1995)
- [9] F. Kun and H.J. Herrmann, "A study of fragmentation process using a discrete element method" *Comput. Methods Appl. Mech. Engrg.* **138**, 3-18 (1996)
- [10] G. A. Addetta, F. Kun, E. Ramm, "On the application of a discrete model to the fracture process of cohesive granular materials" *Granular Matter* **4**, 77-90 (2002)
- [11] F. Kun and H. J. Herrmann, *Fragmentation of Colliding Discs*, *Int. Jour. Mod. Phys. C* **7**, pp. 837-855 (1996).
- [12] F. Kun and H. J. Herrmann, "Transition from damage to fragmentation in collision of solids", *Phys. Rev. E* **59**, 2623 (1999).
- [13] F. Alonso-Marroquin and H. J. Herrmann, "Calculation of the incremental stress-strain relation of a polygonal packing", *Phys. Rev. E* (2002) in press.
- [14] K. Bagi, "Microstructural Stress Tensor of Granular Assemblies with Volume Forces" *Journal of Applied Mechanics* **66**, 4 934-936
- [15] N.P. Kruyt and L. Rothenburg, "Micro-mechanical Definition of the strain tensor for granular materials" *ASME Journal of Applied Mechanics* **118**, 706-719 (1996)
- [16] Y. F. Dafalias and E. P. Popov. "Plastic Internal Variables formalism of Cyclic Plasticity" *Journal of Applied Mechanics* **43** 645-650 (1976)
- [17] F. Tatsuoka and K. Ishihara, "Yielding of sand in triaxial compression" *Soil and Foundations* **14**, 2 63-76 (1974)
- [18] D.C. Drucker and W. Prager. "Soil Mechanics and plastic analysis of limit design", *Q. Applied Math.* **10**(2) 157-165 (1952)
- [19] M. Lätzel, S. Luding, and H. J. Herrmann, "Macroscopic material properties from quasi-static, microscopic simulations of a two-dimensional shear-cell" *Granular Matter* **2**(3), 123-135, (2000)